

Fig. 6. Length of second resident time vs substrate temperature for 33L glass containing 30% crystallization.

temperatures, under the influence of the electric field created by the electron beam.

The rate of signal decay is not only dependent on the beam current and substrate temperature but is also strongly dependent on the

microstructure of the material. The presence of crystals in the glass matrix produces a second resident time. During this period the local temperature increases to a value where migration of Li ions in the crystalline phase can occur under the influence of the electron-beam-induced electric field.

Both the change in decay rates and the presence of the second resident time may provide a basis for performing microstructural as well as compositional analyses.

**Acknowledgments:** The writers thank P. H. Holloway and C. G. Pantano, Jr. for helpful discussions and M. Ogino for technical assistance.

## References

- C. G. Pantano, Jr., D. B. Dove, and G. Y. Onoda, Jr., "AES Compositional Profiles of Mobile Ions in the Surface Region of Glass," *J. Vac. Sci. Technol.*, **13**[1] 414-18 (1976).
- S. Thomas, "Electron-Irradiation Effect in the Auger Analysis of SiO<sub>2</sub>," *J. Appl. Phys.*, **45** [1] 161-66 (1974).
- P. T. Dawson, O. S. Heavens, and A. M. Pollard, "Glass Surface Analysis by Auger Electron Spectroscopy," *J. Phys. C: Solid State Phys.*, **11**, p. 2183 (1978).
- C. G. Pantano, Jr., D. B. Dove, and G. Y. Onoda, Jr., "AES Analysis of Sodium in a Corroded Bioglass Using a Low Temperature Technique," *Appl. Phys. Lett.*, **26** [11] 601-602 (1975).
- L. L. Hench, S. W. Freiman, and D. L. Kinser, "Early Stages of Crystallization in an Li<sub>2</sub>O-2SiO<sub>2</sub> Glass," *Phys. Chem. Glasses*, **12** [2] 58-63 (1971).
- L. A. Harris, "Analysis of Materials by Electron-Excited Auger Electrons," *J. Appl. Phys.*, **39** [3] 1419-27 (1968).
- C. E. Holcombe, Jr., G. L. Powell, and R. E. Clausing, "Low-Energy Electron Diffraction and Auger Emission Spectroscopy Studies of Lithium Hydride (100) Surface," *Surf. Sci.*, **30** [3] 561-72 (1972).
- T. M. El-Shamy and C. G. Pantano, Jr., "Decomposition of Silicate Glasses in Alkaline Solutions," *Nature*, **266** [5604] 704 (1977).
- T. E. Gallon and J. A. D. Matthew, "Low-Energy Auger Emission from Lithium Fluoride," *Phys. Status Solidi B*, **41** [1] 343-51 (1970).
- W. D. Kingery, H. K. Bowen, and D. R. Uhlmann, *Introduction to Ceramics*. Wiley & Sons, New York, 1976.

# Quenched Metastable Glassy and Crystalline Phases in the System Lithium-Sodium-Potassium Metaniobate-Tantalate

KURT NASSAU, CHRISTINE A. WANG,\* and MICHAEL GRASSO

Bell Laboratories, Murray Hill, New Jersey 07974

A previous study of the system (Li,Na,K)TaO<sub>3</sub> was extended to include the metaniobates. Glasses were made by twin-roller-quenching 33 compositions in the three pseudobinary systems as well as in the pseudoternary system composed of LiNbO<sub>3</sub>, NaNbO<sub>3</sub>, and KNbO<sub>3</sub> and in the pseudobinary M(Nb,Ta)O<sub>3</sub> where M is Li, Na, or K. Glasses were obtained in all but the most Na-rich regions. Study of these metastable compositions by X-ray diffraction and differential thermal analysis showed the appearance of four metastable crystalline phases on crystallization, one centered at KNbO<sub>3</sub>, one with an extended occurrence in the ternary system (Li,Na,K)NbO<sub>3</sub>, one centered about Li<sub>0.6</sub>Na<sub>0.4</sub>NbO<sub>3</sub>, and one at KNb<sub>0.25</sub>Ta<sub>0.75</sub>O<sub>3</sub>. There is some evidence for a subsolidus two-glass region in the system (K,Na)NbO<sub>3</sub>. The ionic conductivity of the LiNbO<sub>3</sub> glass was  $\approx 10^{-5} \Omega^{-1} \text{cm}^{-1}$  and the dielectric constant shows ferroelectricity-like behavior. Some infrared absorption data gave almost identical curves for the glass and the metastable crystalline phase, which was the first to crystallize.

## I. Introduction and Experimental Procedure

**M**ETASTABLE phases in the system (Li,Na,K)TaO<sub>3</sub> were described previously.<sup>1</sup> Glass was observed on twin-roller-quenching in all but the sodium-rich corner of the pseudoternary phase diagram and, when heated, two metastable crystalline phases, designated *M* and *N*, formed in a large region about KTaO<sub>3</sub> and near Li<sub>0.8</sub>K<sub>0.2</sub>TaO<sub>3</sub>, respectively. Some early references on quenching are also given there.

The present report extends the study to the three pseudobinary systems and the pseudoternary systems involving LiNbO<sub>3</sub>, NaNbO<sub>3</sub>, and KNbO<sub>3</sub>, as well as the pseudobinary niobate-tantalate systems of Li, Na, and K.

The experimental and interpretive techniques are identical to those reported previously.<sup>1</sup> Infrared data were run on a spec-

Received July 12, 1978; revised copy received November 16, 1978.

\*Now with the Massachusetts Institute of Technology, Cambridge, Massachusetts 02139.

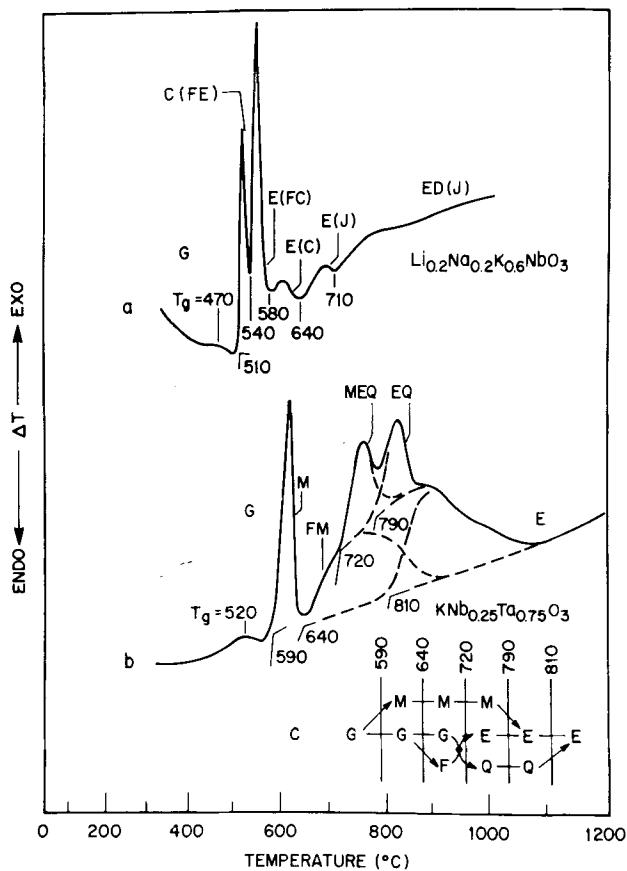


Fig. 1. DTA curves taken at 20°/min in flowing  $\text{N}_2$  of (a)  $\text{Li}_{0.2}\text{Na}_{0.2}\text{K}_{0.6}\text{NbO}_3$  and (b)  $\text{KNb}_{0.25}\text{Ta}_{0.75}\text{O}_3$ , as well as (c) the transformation sequence inferred for the latter.

trophotometer\* at room temperature using both flakes as well as KBr pellets with KBr in the reference beam.

## II. Results

Figure 1 shows typical differential thermal analysis (DTA) results for the compositions studied. Letters designate phases as described below. The range of sharp and broad exotherms was interpreted as was done previously.<sup>1</sup> Powder X-ray diffraction (XRD) patterns were taken after each peak, with additional samples within broad peaks. A particularly complex DTA curve was the  $\text{KNb}_{0.25}\text{Ta}_{0.75}\text{O}_3$  curve of Fig. 1(b). Five separate exotherms were inferred from the diffraction data; the sequence of phase transformations deduced from this data is shown in Fig. 1.

The data for the niobate systems are given in Table I; Fig. 2 shows the phase transformation diagrams<sup>1</sup> for the three pseudobinary systems. For the pseudoternary system, Fig. 3 shows the range of occurrence of the metastable phases; there are the glass *G* and three new crystalline metastable phases designated *C*, *F*, and *H*.

Data for the mixed niobate-tantalate pseudobinary systems are given in Table II and the phase transformation diagrams for the glasses obtained are shown in Fig. 4. Here *Q* designates yet another new crystalline metastable phase.

## III. Discussion

### (1) Glass Formation and the Quenching Rate

Many criteria have been proposed to explain why some compositions can be quenched to a glass and others cannot, as for example the number of oxygens per cation and the radius ratio of the cations.<sup>2</sup> The best approach appears to be that of Takamori and Roy,<sup>3</sup> who postulated that a noncrystalline solid, if not a glass, can always be formed at a high enough quench rate as long as the final temperature is below that for glass crystallization. Using an analogous approach, Uhlmann<sup>4</sup> treated the homogeneous crystallization of single-component materials and gave several relevant references. From

\*Model 283, Perkin-Elmer Corp., Norwalk, Conn.

Table I. Niobate Compositions Quenched and Thermal Transformations

| Composition (mol%) |                    |                   | Quench conditions |     | Thermal transition sequence <sup>†</sup>   |
|--------------------|--------------------|-------------------|-------------------|-----|--|
| LiNbO <sub>3</sub> | NaNbO <sub>3</sub> | KNbO <sub>3</sub> | Temp.* (°C)       | No. |  |
| 100                |                    |                   | 1550              | 6   | <i>G</i> 460–490 <i>J</i>  |
|                    | 100                |                   | 1410–1700         | 10  | Crystal only   |
|                    |                    | 100               | 1225              | 3   | <i>G</i> 380 <sup>‡</sup> 460–510 <i>F</i> 690–740 <i>E</i>  |
| 80                 | 20                 |                   | 1375              | 1   | <i>G</i> { <i>H</i> } 480 <i>HJ</i> 500–830 <sup>§</sup> <i>J</i> ( <i>E</i> )   |
| 60                 | 40                 |                   | 1250              | 4   | <i>G</i> ( <i>H</i> ) 520 <i>H</i> ( <i>J</i> )– <i>JE</i> ( <i>H</i> ) 850 <sup>§</sup> <i>J</i> ( <i>E</i> )   |
| 40                 | 60                 |                   | 1400              | 1   | <i>GH</i> 440 <i>HE</i> 520 <i>HE</i> ( <i>J</i> )– <i>E</i> ( <i>HJ</i> ) 840 <sup>§</sup> <i>EJ</i>  |
| 20                 | 80                 |                   | 1350–1850         | 7   | Crystal only   |
|                    | 80                 | 20                | 1650              | 5   | <i>E</i> ( <i>G</i> ) 500 <i>E</i> (little glass only)   |
|                    | 70                 | 30                | 1360              | 1   | <i>GE</i> 510 <i>E'</i> 550 <i>E'</i> ( <i>CF</i> ) 640–710 <i>E'C</i> 670–770 <i>E</i>  |
|                    | 60                 | 40                | 1330              | 2   | <i>G</i> 500 <sup>‡</sup> 520 <i>E'</i> 550 <i>E'</i> ( <i>CF</i> ) 620–680 <i>E'C</i> 670–840 <i>E</i>  |
|                    | 40                 | 60                | 1350              | 2   | <i>G</i> 500 <sup>‡</sup> 520 <i>E'</i> 550 <i>E'</i> ( <i>CF</i> ) 600–730 <i>E'C</i> 680– <i>E'E</i> –790 <i>E</i>   |
|                    | 20                 | 80                | 1350              | 1   | <i>G</i> 500 <sup>‡</sup> 530 <i>F</i> 550 <i>FE'</i> 590–690 <i>FE'C</i> 670–850 <i>E</i>   |
| 10                 |                    | 90                | 1275              | 2   | <i>G</i> 450 <sup>‡</sup> 550 <i>F</i> 620 <i>ED</i>   |
| 20                 |                    | 80                | 1300              | 1   | <i>G</i> 490 <sup>‡</sup> 510 <i>F</i> 530 <i>C</i> ( <i>F</i> ) 600–620 <i>CE</i> 650–680 <i>ED</i>   |
| 30                 |                    | 70                | 1350              | 1   | <i>G</i> 520 <sup>‡</sup> 540 <i>C</i> ( <i>F</i> ) 590–610 <i>CE</i> 660–680 <i>DE</i>  |
| 40                 |                    | 60                | 1300              | 1   | <i>G</i> 510 <sup>‡</sup> 530 <i>C</i> 630–670 <i>D</i>  |
| 50                 |                    | 50                | 1350              | 1   | <i>G</i> 510 <i>G</i> 540 <i>C</i> 630–650 <i>D</i> ( <i>J</i> )   |
| 60                 |                    | 40                | 1350              | 1   | <i>G</i> 490–540 <i>G</i> 550 <i>C</i> 610 <i>CD</i> 650 <i>DJ</i>   |
| 80                 |                    | 20                | 1425              | 3   | <i>G</i> 500 <i>G</i> 520 <i>G</i> 570 <i>JC</i> 610–690 <i>JD</i>   |
| 90                 |                    | 10                | 1375              | 2   | <i>G</i> 520 <i>J</i> ( <i>D</i> )   |
| 33.3               | 33.3               | 33.3              | 1400              | 1   | <i>G</i> 510 <sup>‡</sup> 530 <i>ED</i> 650–700 <i>EDJ</i>   |
| 20                 | 20                 | 60                | 1350              | 1   | <i>G</i> 470 <sup>‡</sup> 510 <i>C</i> ( <i>FE</i> ) 540 <i>E</i> ( <i>FC</i> ) 580 <i>E</i> ( <i>C</i> ) 640 <i>E</i> ( <i>J</i> ) 710–770 <i>ED</i> ( <i>J</i> ) |
| 20                 | 60                 | 20                | 1500              | 1   | <i>G</i> ( <i>E</i> ) 500 <i>E</i> 520 <i>E</i> ( <i>D</i> )– <i>E</i> ( <i>JD</i> ) 900 <sup>§</sup> <i>EJD</i>   |
| 60                 | 20                 | 20                | 1400              | 1   | <i>G</i> 510 <i>EC</i> 560 <i>JDE</i>  |

\*Quench temp. for best glass is given; if crystal only, full range tried is given. †Symbols given in estimated order of amount present: ( ) indicates small amount, { } indicates partial X-ray pattern only. Transitions are exotherms except for glass transitions marked ‡; major peaks underlined; temperatures in °C; § indicates change in slope only.

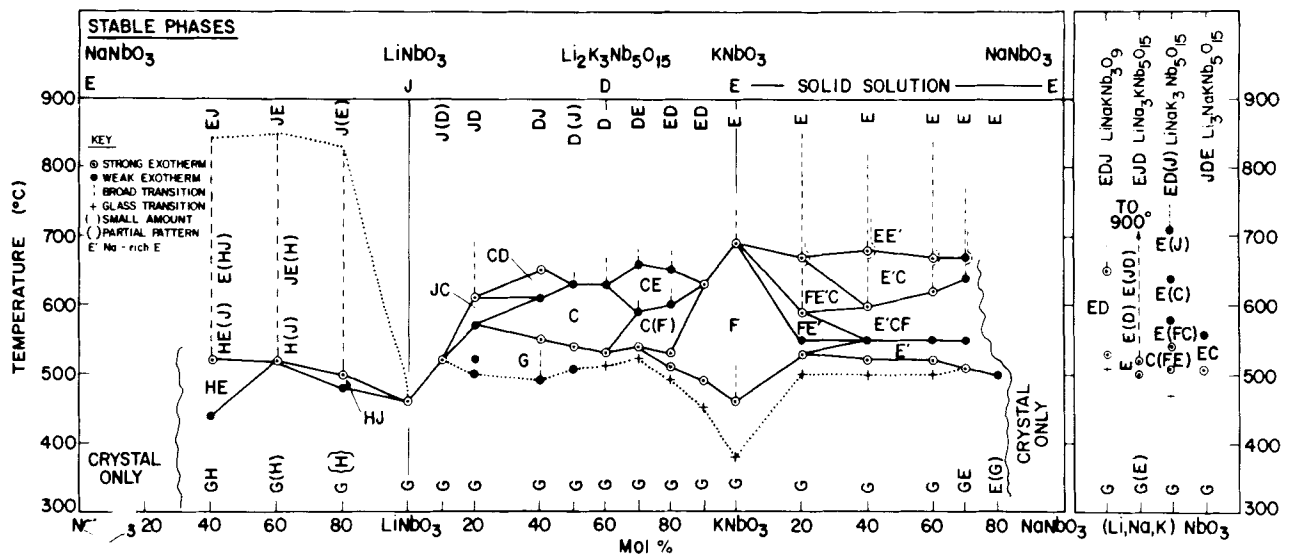


Fig. 2. Phase transformation diagrams for quenched glasses in the system (Li,Na,K)NbO<sub>3</sub>.

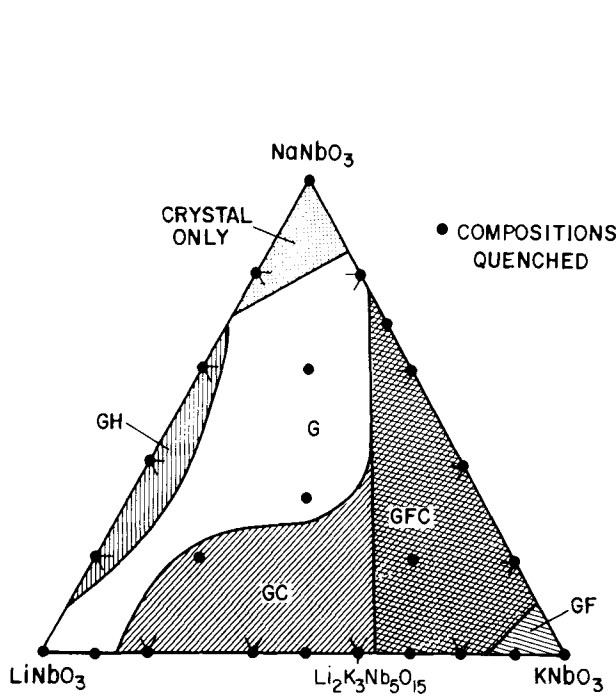


Fig. 3. Occurrence of metastable phases in the system (Li,Na,K)NbO<sub>3</sub>; G indicates glass; C, F, and H are metastable crystalline phases.

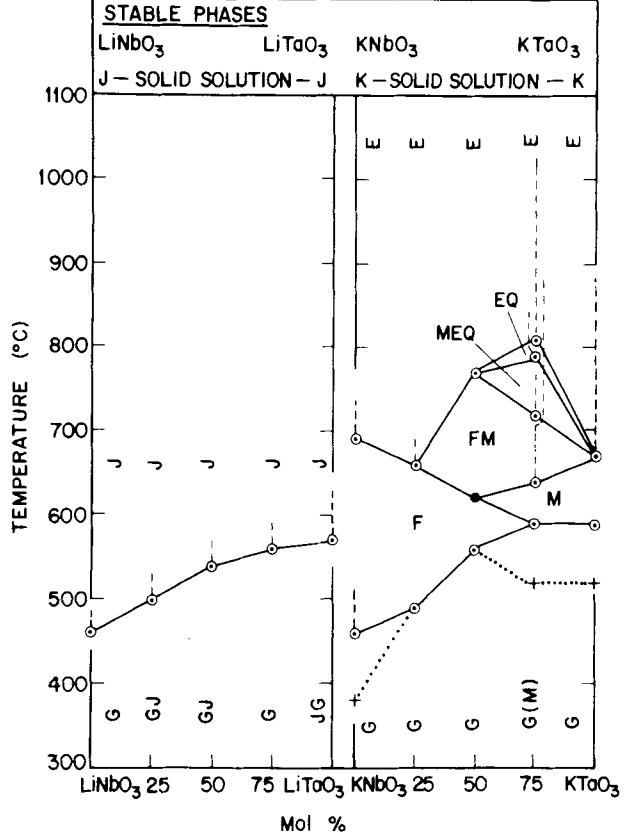


Fig. 4. Phase transformation diagrams for quenched glasses in the pseudobinary systems Li(Nb,Ta)O<sub>3</sub> and K(Nb,Ta)O<sub>3</sub>; see Fig. 2 for key.

Table II. Mixed Niobate-Tantalate Compositions Quenched and Thermal Transformations\*\*

| X  | Composition (mol%) |                   | Quench conditions |     | Thermal transition sequence          |
|----|--------------------|-------------------|-------------------|-----|--------------------------------------|
|    | XNbO <sub>3</sub>  | XTaO <sub>3</sub> | Temp.* (°C)       | No. |                                      |
| Li | 75                 | 25                | 1575              | 2   | GJ 500-530 J                         |
|    | 50                 | 50                | 1550              | 2   | GJ 540-570 J                         |
|    | 25                 | 75                | 1725              | 4   | G 560-590 J                          |
|    | 0                  | 100               | 1850              | 7   | JG 570-630 J                         |
| Na | 75                 | 25                | 1600-1800         | 2   | Crystal only                         |
|    | 50                 | 50                | 1700-1900         | 3   | Crystal only                         |
|    | 25                 | 75                | 1800-2000         | 3   | Crystal only                         |
|    | 0                  | 100               | 1850-1950         | 4   | Crystal only                         |
| K  | 75                 | 25                | 1275              | 1   | G 490 F 670-690 E                    |
|    | 50                 | 50                | 1320              | 1   | G 560 F 620 FM 770 E                 |
|    | 25                 | 75                | 1375              | 2   | G {M} 520* 590 M 640-880 FM 720-770† |
|    | 0                  | 100               | 1450              | 3   | G {M} 520* 600 M 670 ME-E(M) 890 E   |

\*\*See Table I for symbols. †Continuation: MEQ 790-830 EQ 880-1030E.

this point of view the important factor is not a configuration favoring a glass structure, but a state discouraging rapid crystallization under the quench conditions available, i.e. a high melt viscosity and low nucleation and crystal growth rates.

The quench rate was estimated for the quenching of  $\text{KNbO}_3$ . The material entering the rollers is between the measured melt temperature ( $1320^\circ$ ) and the melting point ( $1040^\circ\text{C}$ ). The emerging flakes are  $<460^\circ\text{C}$ , the temperature at which crystallization occurs. By measuring the heat transferred by quenched flakes emerging from the rollers into an oil-filled calorimeter, a final temperature of  $200 \pm 15^\circ\text{C}$  was established. The quenching temperature range may thus be taken as  $\approx 1000^\circ\text{C}$ .

The trajectory of the flakes is fairly direct from between the rollers, with little evidence of sticking. This pattern can be attributed in part to the very high centrifugal force, which at 3000 rpm is calculated to be  $\sim 1000g$  ( $G$  being the earth's gravity). Sarjeant and Roy<sup>5</sup> observed that in conventional splat cooling techniques the oxides do not wet metals but bounce off. All that remains is to establish the contact time during which quenching occurs. The rotation rate of 3000 rpm corresponds to a linear velocity of 785 cm/s. A reasonable estimate of the contact time can be derived from the distance from roller contact to a spacing of  $20\ \mu\text{m}$ , the maximum thickness of relatively thick flakes. For 2.5-cm-radius rollers, this distance is 0.071 cm, corresponding to a contact time of  $8.9 \times 10^{-5}$  s and yielding a quench rate of  $1.1 \times 10^7$  degrees/s. The lower thickness of  $10\ \mu\text{m}$ , which is often observed, would increase this calculated quench rate, whereas a short sticking distance would decrease it.

Since at the end of even a 10-g quench the rollers are merely warm, cooling them would add little to the effective quench rate in comparison with the high initial melt temperature.

Alternative ways of calculating quench rates have been presented in the literature, but not all of the assumptions in any approach are necessarily valid.

Following the approach of Ruhl,<sup>6</sup> the thermal conductivity  $k$  can be used to calculate heat transfer for ideal cooling in a flake of thickness  $l$  to give the final central temperature  $T_f$  in a flake from an initial melt at  $T_m$  and a roller temperature of  $T_r$  as

$$T_f = T_r + (T_m - T_r) \exp[-kt/(c^2 d)] \quad (1)$$

where  $c$  is the heat capacity at constant pressure,  $t$  the time in seconds, and  $d$  the density. For Newtonian cooling,  $k$  is replaced by  $hd$  where  $h$  is the heat-transfer coefficient. This equation yields an average cooling rate to one-half temperature of  $(dT/dt) = 8.2 \times 10^6$  degrees/s for ideal and  $7.1 \times 10^4$  degrees/s for Newtonian cooling for a typical compound oxide, such as  $\text{KNbO}_3$ , onto an iron substrate using the Sarjeant and Roy<sup>5</sup> estimate that  $k$  is approximately ten times the thermal conductivity. It is expected that actual cooling is intermediate, i.e. near  $10^6$  degrees/s.

Suzuki and Saito<sup>8</sup> and Sarjeant and Roy<sup>7</sup> calculated the growth rate from a preexisting nucleus; a glass is formed if quenching is too rapid for the nucleus to grow successfully. Suzuki and Saito used

$$(dT/dt) = [(ZH^2)/(dcT_m\eta V^{5/3})] \quad (2)$$

where  $H$  is the enthalpy of fusion,  $\eta$  the viscosity,  $V$  the molar volume, and  $Z$  a constant calculated<sup>8</sup> for a silicate having a viscosity of 32 P. Correcting this to an estimated 0.1 P for  $\text{KNbO}_3$  gives  $(dT/dt) = 3.0 \times 10^7$  degrees/s to prevent growth of a 5-nm nucleus. The analogous treatment of Sarjeant and Roy<sup>7</sup> uses  $(dT/dt) = [2 \times 10^{-6}(T_m^2 R)/V\eta]$  where  $R$  is the gas constant. Recalculating for a change in viscosity gives  $(dT/dt) = 9.6 \times 10^6$  degrees/s to prevent growth of a 1-nm nucleus. It appears that a quenching rate of  $\approx 10^7$  degrees/s is present in the quenching of the oxides studied.

## (2) The Occurrence of Glass

The basis on which the designation  $G$  for glass is assigned was discussed previously<sup>1</sup>; to this basis can now be added the development of  $\text{Cr}^{3+}$  fluorescence in  $\text{LiNbO}_3$  on crystallization. Glass is observed at all but the most Na-rich concentrations (Figs. 2 and 3), as in the tantalate system.

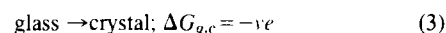
Glass transitions are observed more widely than in the tantalate system and, over most of the region, appeared as the usual second-order phase transition showing a small endotherm and resulting in a

change in slope (Fig. 1). However, in  $\text{Li}_{0.6}\text{K}_{0.4}\text{NbO}_3$  and  $\text{Li}_{0.5}\text{K}_{0.5}\text{NbO}_3$  a small exotherm appeared instead. Examination after such an exotherm and before the following crystallization exotherm showed that crystallization had not yet occurred. It appears that heat is evolved during such a glass transition when enough excess energy is quenched into the glass. In the glass of composition  $\text{Li}_{0.8}\text{K}_{0.2}\text{NbO}_3$ , two small exothermic glass transitions were observed before crystallization. This finding may indicate a two-glass region with each glass having its own  $T_g$ , but with only a single crystallization temperature. It was not further investigated.

The tantalates of the previous study<sup>1</sup> were quite stable to ambient exposure; in the case of the niobates, however, considerable atmospheric reaction occurred. A sample of quenched  $\text{LiNbO}_3$ , after one year of ambient storage, showed significant OH and  $\text{CO}_2$  in the ir absorption bands. Heating for 5 min at  $250^\circ\text{C}$  removed some of the contaminants, but subsequent soaking for 10 min in room-temperature water removed all the  $\text{CO}_2$  and only slightly increased the OH, confirming that these effects are surface, not bulk.

In the case of niobate glasses containing significant amounts of potassium (the most reactive of the alkali metals used), complete deterioration of the glass flakes by hydration occurred in hours or days and specimens were accordingly stored in a desiccator. It appears that the glass is disordered enough that some surface K ions in their oxygen environment do not experience their niobate neighbors strongly enough and thus react with the ambient moisture and  $\text{CO}_2$ , as  $\text{K}_2\text{O}$  would, rather than as  $\text{KNbO}_3$ . The crystalline  $F$  phase also hydrated rapidly whenever significant  $\text{KNbO}_3$  was present. The  $F$  phase reacted with the acetone collodion used to mount powders for XRD analysis, so adhesive tape had to be used.

This hydration phenomenon can also be considered from a free energy point of view. Consider the crystallization of a glass of such a composition that the resultant crystalline material does not hydrate in the ambient atmosphere. Assuming that these are equilibrium considerations and that there are no kinetic barriers, the Gibbs free energy values,  $\Delta G$ , are implied:



with subscripts  $g$ ,  $c$ , and  $h$  standing for glass, crystal, and hydrate.

In the direct hydration of the glass



the initial and final states are the same as those in Eqs. (3) and (4), respectively, so that

$$\Delta G_{g,h} = \Delta G_{g,c} + \Delta G_{c,h} \quad (6)$$

If then the magnitude of the negative  $\Delta G_{g,c}$  is larger than that of the positive  $\Delta G_{c,h}$ ,  $\Delta G_{g,h}$  will become negative and the glass will hydrate even if the crystal does not. Kinetic factors could also be involved.

Sarjeant and Roy<sup>5</sup> noted glass formation in the 30 to 80%  $\text{Nb}_2\text{O}_5$  range of the systems  $\text{K}_2\text{O-Nb}_2\text{O}_5$  and  $\text{Na}_2\text{O-Nb}_2\text{O}_5$ , but gave no details other than the ir spectra of  $\text{KNbO}_3$ . Kokubo *et al.*<sup>9</sup> and Ito *et al.*<sup>10</sup> reported a mixed niobate-tantalate glass composition.

## (3) Stable Crystalline Phases

The stable phases are shown at the top of Fig. 2; since all involve ferroelectricity, detailed summaries and many references may be found compiled in Ref. 11. Relevant phase-diagram studies have also appeared for the systems  $(\text{Li},\text{Na})\text{NbO}_3$ ,<sup>12</sup>  $(\text{Na},\text{K})\text{NbO}_3$ ,<sup>13</sup> and  $(\text{Li},\text{Na})\text{TaO}_3$ .<sup>14</sup> These data may be summarized as:

The perovskite structure occurs for  $\text{NaNbO}_3$  (JCPDS No. 14-603),<sup>15</sup>  $\text{KNbO}_3$  (JCPDS No. 9-156), and the equivalent tantalates as previously discussed,<sup>1</sup> as well as for their solid solutions. Many polymorphs exist for these compounds (as many as five for  $\text{NaNbO}_3$ ) but the powder patterns are very similar in the temperature region studied (splitting of lines is the main effect) and these types of symmetry change were not followed. All phases in this group were designated  $E$ , unless the lattice parameters indicated a composition which was not consistent with the overall composition of the mixture (as reflected by the lattice parameter of a sample heated near

Table III. Structure C

| Li <sub>0.4</sub> K <sub>0.6</sub> NbO <sub>3</sub> at 590°C |                         | Li <sub>0.2</sub> Na <sub>0.2</sub> K <sub>0.6</sub> NbO <sub>3</sub> at 650°C |                         | Na <sub>0.6</sub> K <sub>0.4</sub> NbO <sub>3</sub> at 670°C |                         |
|--|-------------------------|--|-------------------------|--|-------------------------|
| <i>d</i> <sub>obs</sub> (Å)*                                 | <i>l</i> <sub>obs</sub> | <i>d</i> <sub>obs</sub> (Å) <sup>‡</sup>                                       | <i>l</i> <sub>obs</sub> | <i>d</i> <sub>obs</sub> (Å) <sup>‡</sup>                     | <i>l</i> <sub>obs</sub> |
| 8.26   | vvs                     | 8.34   | m                       | 8.55   | vs                      |
| 7.96   | vs                      | 7.96   | vs                      | 5.52   | vw                      |
| 5.56   | vw                      | 5.68   | w                       | 3.83   | s                       |
| 5.10   | mw                      | 3.77   | vs                      | 3.27   | m                       |
| 3.798  | m                       | 3.65   | w                       | 3.207  | m                       |
| 3.530  | mw                      | 3.26   | vw                      | 3.129  | vw                      |
| 3.138  | m                       | 3.14   | s                       | 2.966  | m                       |
| 85   | mw                      | 3.056  | m                       | 2.285  | w                       |
| 3.28   | s                       | 2.634  | m                       | 2.236  | w                       |
| 2.948  | m                       |  |                         |  |                         |
| 2.858  | ms                      |  |                         |  |                         |
| 2.653  | vw                      |  |                         |  |                         |
| 2.460  | w                       |  |                         |  |                         |
| 2.384  | vw                      |  |                         |  |                         |
| 2.224  | vw                      |  |                         |  |                         |
| 1.934  | mw                      |  |                         |  |                         |

\*From corrected Guinier pattern for pure C. <sup>‡</sup>From uncorrected diffractometer traces of mixed phases, where there may be superposition of lines.

melting), in which case *E'* was used to designate Na-rich crystalline phases, as was done previously.<sup>1</sup>

The isostructural LiNbO<sub>3</sub> (JCPDS No. 20-631) and LiTaO<sub>3</sub> (JCPDS No. 9-187), both designated *J*, as well as the tungsten bronzes K<sub>3</sub>Li<sub>2</sub>Ta<sub>5</sub>O<sub>15</sub> (JCPDS No. 23-1198), designated *L*, and K<sub>3</sub>Li<sub>2</sub>Nb<sub>5</sub>O<sub>15</sub>, designated *D*, are the only other stable crystalline phases reported in the system (Li,Na,K)(Nb,Ta)O<sub>3</sub>; no others were observed.

#### (4) Metastable Crystalline Phases

(A) *Phase M*: This pyrochlore phase was also previously reported<sup>1</sup> in the system (Li,Na,K)TaO<sub>3</sub> and occurs here only in K(Nb<sub>1-x</sub>Ta<sub>x</sub>)O<sub>3</sub> for *x* from 0.5 to 1.0 (Fig. 4). This phase appears to be the same as the reported K<sub>1.5</sub>(Ta<sub>0.65</sub>Nb<sub>0.35</sub>)O<sub>5.75</sub> of Kokubo *et al.*<sup>9</sup> and Ito *et al.*<sup>10</sup> As previously discussed,<sup>1</sup> they did not include their observed 2.5% AlO<sub>0.15</sub> and 3.4% SiO<sub>2</sub> content in their formula; we see no need for an oxygen-deficient formulation. The cubic defect pyrochlore<sup>16</sup> cell parameter of KNb<sub>0.25</sub>Ta<sub>0.75</sub>O<sub>3</sub> is 10.61 Å, in good agreement with the 10.62 Å of Kokubo *et al.* and Ito *et al.* and the 10.590 Å for KTaO<sub>3</sub>, for which an indexed powder pattern was given.<sup>1</sup>

(B) *Phase C*: This new metastable phase occurs in the systems Li<sub>x</sub>K<sub>1-x</sub>NbO<sub>3</sub> and K<sub>x</sub>Na<sub>1-x</sub>NbO<sub>3</sub>. Figure 3 shows that these two areas of occurrence are connected by a broad region in the ternary system, not including, however, the KNbO<sub>3</sub> corner. Unlike the other metastable crystalline phases *N*, *M*,<sup>1</sup> and *F*, the diffraction

pattern of *C* changes somewhat; if it were not for a continuous variation over the region of its occurrence (Fig. 3), its identity as a single phase would have been questioned. The *d* spacings for three of the *C* compositions are given in Table III; indexing was not possible.

(C) *Phase F*: This new metastable phase was observed in four regions: in the systems Li<sub>x</sub>K<sub>1-x</sub>NbO<sub>3</sub> and K<sub>x</sub>Na<sub>1-x</sub>NbO<sub>3</sub> (Fig. 2), in the system Li<sub>x</sub>Na<sub>y</sub>K<sub>1-x-y</sub>NbO<sub>3</sub> (Fig. 3), and in the system KNb<sub>x</sub>Ta<sub>1-x</sub>O<sub>3</sub> (Fig. 4). Its existence as a metastable phase of composition-pure KNbO<sub>3</sub> is supported by the observed *d* spacings given in Table IV, which did not vary over its wide range of occurrence; there is, of course, the possibility of some minor alkali solid solubility. It was not possible to index the powder pattern.

Flueckinger *et al.*<sup>17</sup> noted a fleeting primary product during the reaction of K<sub>2</sub>CO<sub>3</sub> and Nb<sub>2</sub>O<sub>5</sub> to form KNbO<sub>3</sub>. This product is present between 380° and 470°C at the very slow heating rate of 0.2°C/min. There is some similarity between their X-ray powder pattern and that of phase *F*, but their pattern contains several additional lines; it is possible that the metastable phase *F* is present with another phase during this reaction.

(D) *Phase H*: This new metastable phase, which was never observed as a single phase, occurs in the system Na<sub>x</sub>Li<sub>1-x</sub>NbO<sub>3</sub> (Fig. 2). The powder pattern (Table IV) was studied in the as-quenched roller-quenched flakes, which showed significant regions of crystallinity but contained no other crystalline phases. It could

Table IV. Structures *F*, *H*, and *Q*

| Structure <i>F</i> , KNbO <sub>3</sub> , at 570°C |                         | Structure <i>H</i> , present in as-quenched flakes of Li <sub>0.6</sub> Na <sub>0.4</sub> NbO <sub>3</sub> |                         | Structure <i>Q</i> , present in KNb <sub>0.25</sub> Ta <sub>0.75</sub> O <sub>3</sub> at 830°C with <i>F</i> lines removed |                         |
|---|-------------------------|--|-------------------------|--|-------------------------|
| <i>d</i> <sub>obs</sub> (Å)*                      | <i>l</i> <sub>obs</sub> | <i>d</i> <sub>obs</sub> (Å)*   | <i>l</i> <sub>obs</sub> | <i>d</i> <sub>obs</sub> (Å)*   | <i>l</i> <sub>obs</sub> |
| 7.87  | m                       | 3.83   | vs                      | 11.3 <sup>†</sup>  | vvs                     |
| 7.37  | vvs                     | 2.759  | s                       | 5.68   | vs                      |
| 7.00  | s                       | 2.652  | m                       | 5.43   | m                       |
| 3.94  | vw                      | 2.589  | vw                      | 5.28   | w                       |
| 3.606   | vw                      | 2.294  | vw                      | 4.33   | vs                      |
| 3.331   | vs                      | 2.177  | vw                      | 5.83   | w                       |
| 3.188   | vs                      | 1.912  | m                       | 3.83   | mw                      |
| 3.144   | vs                      | 1.738  | m                       | 3.26   | vw                      |
| 2.992   | m                       | 1.687  | vw                      | 3.14   | vvs                     |
| 2.828   | mw                      | 1.616  | m                       | 3.09   | s                       |
| 2.620   | w                       | 1.551  | m                       | 2.93   | m                       |
| 2.519   | w                       | 1.533  | mw                      | 2.746  | ms                      |
| 2.471   | vw                      | 1.379  | w                       | 2.613  | s                       |
| 2.386   | mw                      | 1.332  | w                       | 2.590  | vw                      |
| 2.226   | vw                      | 1.224  | w                       | 2.365  | vw                      |
| 2.129   | mw                      |  |                         | 2.279  | vw                      |
| 2.052   | mw                      |  |                         | 2.212  | vw                      |

\*From corrected Guinier patterns. <sup>†</sup>Uncorrected, from diffractometer trace.

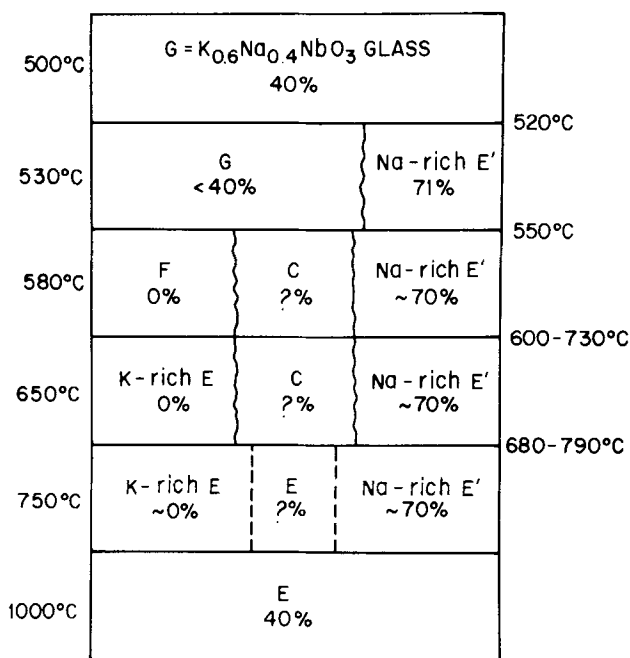


Fig. 5. Transformation of  $K_{0.8}Na_{0.4}NbO_3$  quenched glass with temperature; numbers give the Na content of each phase.

not be established whether the  $d$  spacings varied significantly over the region of existence nor was indexing possible.

(E) Phase Q: This new metastable phase occurred only in one composition studied,  $KNb_{0.25}Ta_{0.75}O_3$  (Fig. 4), and was present with the metastable phase  $M$  and the stable perovskite phase  $E$ . The actual composition of the phase  $Q$  is unknown. The observed  $d$  spacings given in Table IV may not be complete because of possible overlapping of lines in the presence of the other phases; indexing was not possible.

Including phase  $N$ , occurring in the alkali tantalate system,<sup>1</sup> there are six metastable crystalline phases in these systems. It is anticipated that it will be very difficult to prepare single crystals for structural determinations in view of the metastable nature of these phases.

#### (5) Phase Transformations in the System $(Li,Na,K)NbO_3$

The significance of a phase transformation diagram such as that of Fig. 2 and a metastable phase existence diagram such as that of Fig. 3 was discussed<sup>1</sup>; these niobate systems are significantly more complex than the tantalate systems reported.

Glass of the composition  $KNbO_3$  shows a glass transition at 380°, transforms at 460° to the metastable crystalline phase  $F$ , and subsequently converts at 690°C to the stable perovskite phase  $E$ . Both transitions are somewhat broadened, but are still sharp compared to the 210°C wide  $M$ -to- $E$  transformation observed in  $KTaO_3$ . The  $F$  phase has a wide range of occurrence (Fig. 3), but always appears to have the  $KNbO_3$  composition.

In the system  $(K,Na)NbO_3$  phases  $F$  and  $C$  occur with  $E$ , the perovskite  $K_{1-x}Na_xNbO_3$  solid solution. As previously,<sup>1</sup> the multiple distortions from the cubic perovskite are included under the designation  $E$ ; where the X-ray powder diffraction line positions indicated that the initially crystallized  $E$  phase was Na-rich,  $E'$  is used for the Na-rich phase in Table I and Fig. 2. The  $E'$  first crystallizing from the 55% Na glass contained 20% Na, the 71% Na glass 40%, and the 78% Na glass 60%. Using DTA data and X-ray results, the transformation scheme of Fig. 5 can be deduced for  $K_{0.8}Na_{0.4}NbO_3$ . The final phase transition  $C$  and  $E$ , which begins at 680°C as a broad peak, merges into the diffusion-controlled solid-solution  $E$  reaction. At this point several  $E$  and  $E'$  phases of different composition interdiffuse to finally give a single phase of the 40% Na starting composition, which again shows the sharp XRD peaks of the starting powder.

The metastable crystalline phase  $H$  was observed in the region from  $Na_{0.6}Li_{0.4}NbO_3$  to  $Na_{0.2}Li_{0.8}NbO_3$  but was never obtained in pure form. Although the beginning of phase  $H$  disappearance was indicated by a sharp exotherm, not all traces of  $H$  had disappeared until some 320°C later, at which point there was a change in the DTA slope. This very gradual transformation may involve diffusion and would require detailed electron microscopy for clarification. The nature of the remaining transformations in this system can be identified from Figs. 2 and 3 and Table I.

#### (6) Phase Transformations in the Systems $M(Nb,Ta)O_3$

Since mixing of components usually facilitates glass formation, it had been anticipated that glasses might form in the system  $Na(Nb,Ta)O_3$  even though neither end-member would quench to form a glass. However, the end-members are apparently similar enough in their crystallizing characteristics to prevent glass formation (Table II).

The system  $Li(Nb,Ta)O_3$  gave glasses with a monotonously increasing crystallization temperature, where the stable solid solution appeared (Table II and Fig. 4). Glasses formed less readily in this system and only two of the five samples gave essentially pure glass.

Results for the system  $KNb_{1-x}Ta_xO_3$  are also shown in Table II and Fig. 4. Glasses formed readily in this system. The metastable phases  $F$  and  $M$  extended from the end-members to overlap at  $x=0.5$  and 0.75. Although both  $F$  and  $M$  convert to  $E$  with a broad transition elsewhere, the disappearance of a mixture of  $F$  and  $M$  occurs rather surprisingly with a sharp transition in the  $x=0.5$  composition.

The metastable crystalline phase  $Q$  was observed in  $KNb_{0.27}Ta_{0.73}O_3$ . This phase occurred during the four overlapping slow transitions which followed the initial crystallization, as shown in the DTA curve of Fig. 1(b). Analysis of this curve by the examination of more than 20 XRD patterns, taken after heating to various temperatures, permitted the decomposition scheme of Fig. 1(c) to be constructed. It may be assumed that diffusion-controlled reactions are involved to produce these broad transitions; note, for example, that phase  $F$  is expected to have the composition  $KNbO_3$  based on the agreement of the  $d$  spacings with those listed in Table III. It was not possible to detect a variation in the composition of the perovskite  $E$  phase and the actual composition of the  $Q$  phase has not been established unambiguously. Here again, clarification by a detailed electron microscopy study would be needed.

#### (7) Optical Measurements

The ir absorption curves, which demonstrated only a surface reaction of niobate glass with ambient  $H_2O$  and  $CO_2$  were discussed.

Some samples were examined further by ir analysis, where features due to vibrations of the  $NbO_6$  units would be expected to dominate in the 900- to 300- $cm^{-1}$  region. Figure 6(A) shows the spectra of glassy and crystalline  $LiNbO_3$ . The crystalline curve is consistent with the data of Barker and Loudon,<sup>18</sup> who interpreted their ir reflection and Raman spectra on the basis of 11 fundamental modes between 152 and 628  $cm^{-1}$  and combinations near 680  $cm^{-1}$ . The glass curve of Fig. 6(A) is quite different from the crystal curve.

In the case of  $KNbO_3$ , Fig. 6(B) shows the data for the glass, for the metastable  $F$  form which crystallizes from the glass at 460°, and for the stable  $E$  form which appears at 690°C. Here again the stable crystalline spectrum is consistent with the published reflection and Raman data of Bozini and Hurrell.<sup>19</sup> Both the stable crystal  $E$  and the glassy spectra of Fig. 6(B) are consistent with the spectra given by Sarjeant and Roy,<sup>5</sup> who did not, however, note the existence of a metastable crystalline phase.

Most surprising was the fact that there was a close similarity between the glass and the metastable  $F$ -phase curves, whereas the stable phase- $E$  curve was significantly different. The same circumstances were found for the glassy, metastable  $C$  and stable  $D$  forms of  $K_{0.6}Li_{0.4}NbO_3$  (Fig. 6(C)).

To ensure that the glass had not reacted with the KBr pellets, the glass curve of Fig. 6(C) was rechecked using CsBr. There was no change. Also, specimens were hand-picked to ensure the absence of crystal-containing flakes in the glass specimens. It has often been noted that ir- and Raman-active features of stoichiometric crystalline phases somewhat resemble those that occur in the equivalent

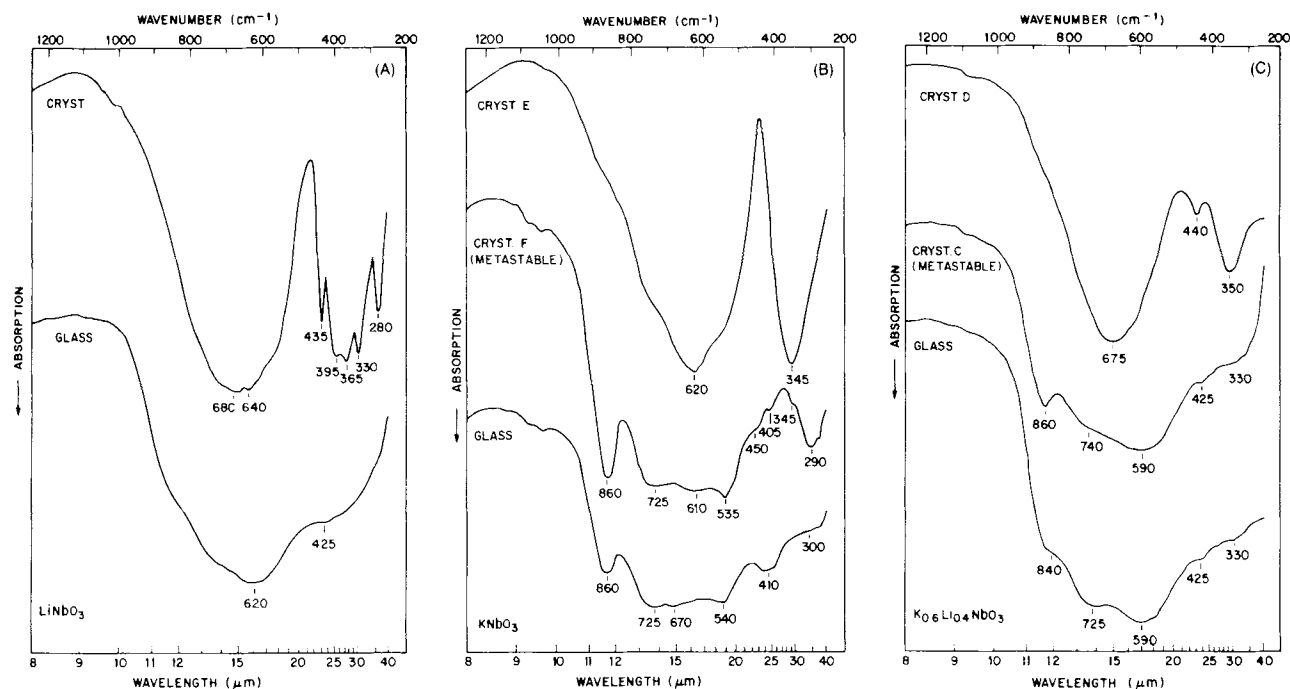


Fig. 6. Infrared absorption curves for KBr pellets of (A)  $\text{LiNbO}_3$ , (B)  $\text{KNbO}_3$ , and (C)  $\text{K}_{0.6}\text{Li}_{0.4}\text{NbO}_3$ .

glass compositions, e.g. for borosilicates by Konijnendijk<sup>20</sup> and Konijnendijk and Stevels<sup>21,22</sup> and for germanates, phosphosilicates, and borates by Bagley *et al.*<sup>23</sup> In all these instances there do not seem to have been intermediate metastable phases.

When an intermediate metastable form does exist, as in Figs. 6(B) and 6(C), it appears that the structural vibrations leading to absorption can be very similar in the glass and the metastable phase, indicating a strong relation in the short-range configurations. These configurations are quite different, however, from those of the stable crystal. Figures 6(B) and 6(C) indicate that this difference may reside in disorder, lower local symmetry, and/or a larger unit cell in the metastable forms, leading to an increase in the number of normal modes and multiple overlapping absorption bands.

The crystallization kinetics of vitreous  $\text{LiNbO}_3$  containing 0.2% Cr was studied by Negran,<sup>24</sup> who used a pulsed laser (6000 Å) to stimulate the ir fluorescence of  $\text{Cr}^{3+}$ . There was little fluorescence in the glass and he followed its intensification in samples which had been heated for various periods at four temperatures from 436° to 493°C. The data gave an activation energy for crystallization of 2.2 eV. The residual fluorescence in the vitreous sample corresponded to only 2% crystallinity, which again confirms the vitreous nature, since even the microcrystalline state would be expected to show the fluorescence.

#### (8) Electrical Measurements

Dielectric measurements<sup>25</sup> (as a function of temperature) on glassy  $\text{LiNbO}_3$  showed two peaks, the upper of which corresponded to the crystallization step, as seen by comparison with the DTA curve in Fig. 7. The anomalous low-temperature peak was unexpected, as were the exceptionally high dielectric constant values, which were  $>10^5$  as measured at 1 kHz at 350° and 500°C, with a significant reduction at 1 MHz.

Such high and dispersive values are characteristic of disordered ferroelectrics with diffuse phase transitions; it was also found that a macroscopic polarization, demonstrating pyroelectricity, could be induced by poling in an electric field while cooling through the lower peak. Nevertheless, ferroelectricity cannot be unambiguously claimed,<sup>25,26</sup> since there is also present a high ionic conductivity presumably deriving from localized motion of the small alkali ions in the glassy matrix, which complicates any interpretation.

For glassy  $\text{LiNbO}_3$  the room-temperature value of the ionic conductivity is  $\approx 10^{-5} \Omega^{-1} \text{cm}^{-1}$ , a value some  $10^{20}$  times greater than

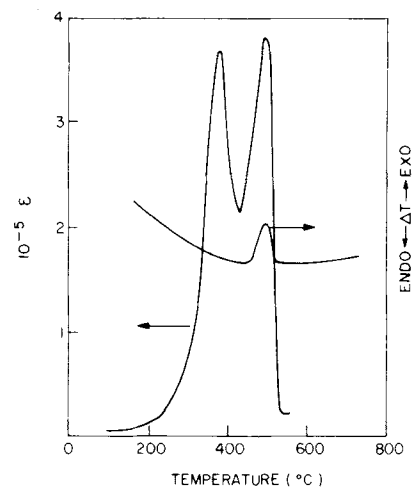


Fig. 7. Dielectric constant and DTA curves of  $\text{LiNbO}_3$ .

that of the single crystal, with an activation energy of 0.40 eV. Small deviations in stoichiometry and small additions of  $\text{WO}_3$  increased the ionic conductivity somewhat, but larger changes and other additions had a deleterious effect.<sup>27</sup> These conductivity values are large enough for possible application as a solid electrolyte in storage batteries.<sup>28</sup>

#### IV. Summary

Together with the previous study<sup>1</sup> of the system  $(\text{Li,Na,K})\text{TaO}_3$  this work provides a systematic survey of the occurrence of quenched glass in the system  $(\text{Li,Na,K})(\text{Nb,Ta})\text{O}_3$ . Glass was obtained in all but the most Na-rich areas. On heating, six metastable crystalline phases were obtained (five for the first time) forming in accordance with Ostwald's step rule on heating the metastable glass and ultimately converting into the expected stable phase assemblages on further heating. Some of these transitions were slow and diffusion-controlled. Metastable two-glass subsolidus regions apparently occur in the systems  $(\text{K,Na})\text{TaO}_3$  and  $(\text{K,Na})\text{NbO}_3$ . The

ionic conductivity of the  $\text{LiNbO}_3$  glass was  $\approx 10^{-5} \Omega^{-1} \text{cm}^{-1}$  and the dielectric constant shows ferroelectric-like behavior. Some ir absorption data gave almost identical curves for the glass and the metastable crystalline phase which was the first to crystallize.

**Acknowledgments:** The writers thank B. E. Prescott for the ir spectra, R. L. Barns for the use of a Guinier camera, J. W. Shiever for assistance with some of the sample preparation, T. Negran, B. Bagley, and A. M. Glass for permission to use their optical and electrical data, and B. Bagley, C. R. Kurkjian, and A. M. Glass for helpful discussions.

## References

- <sup>1</sup> K. Nassau, C. A. Wang, and M. Grasso, "Quenched Metastable Glassy and Crystalline Phases in the Lithium-Sodium-Potassium Metatantalate Pseudoternary System," *J. Am. Ceram. Soc.*, **62** [1–2] 1–4 (1979).
- <sup>2</sup> T. Suzuki and A.-M. Anthony, "Rapid Quenching in the Binary Systems of High-Temperature Oxides," *Mater. Res. Bull.*, **9** [6] 745–53 (1974).
- <sup>3</sup> T. Takamori and R. Roy, pp. 173–82 in *Advances in Nucleation and Crystallization in Glasses*, Edited by L. L. Hench and S. W. Freiman, American Ceramic Society, Columbus, Ohio, 1971.
- <sup>4</sup> D. R. Uhlmann, "Kinetic Treatment of Glass Formation," *J. Non-Cryst. Solids*, **7** [4] 337–48 (1972).
- <sup>5</sup> P. T. Sarjeant and R. Roy, pp. 725–33 in *Sixth International Symposium on the Reactivity of Solids*, Edited by J. W. Mitchell, R. C. DeVries, R. W. Roberts, and P. Cannon, Wiley & Sons, New York, 1969.
- <sup>6</sup> R. C. Ruhl, "Cooling Rates in Splat Cooling," *Mater. Sci. Eng.*, **1** [6] 313–20 (1967).
- <sup>7</sup> P. T. Sarjeant and R. Roy, "New Approach to the Prediction of Glass Formation," *Mater. Res. Bull.*, **3** [3] 265–79 (1968).
- <sup>8</sup> T. Suzuki and S. Saito, "Rate of Heat Liberation by Crystallization as a Resistance to Glass Forming," *ibid.*, **11** [2] 221–25 (1976).
- <sup>9</sup> T. Kokubo, S. Ito, and M. Tashiro, "Formation of a Metastable Pyrochlore-Type Crystal in Glasses," *Bull. Inst. Chem. Res., Kyoto Univ.*, **51** [5] 315–28 (1973).
- <sup>10</sup> S. Ito, T. Kokubo, and M. Tashiro, "Formation of a Metastable Pyrochlore-Type Crystal in  $\text{K}(\text{Ta}, \text{Nb})\text{O}_3$ -Containing Glasses and its Relation to Structure of the Glasses," *Yogyo Kyokai Shi*, **81** [8] 327–33 (1973).

- <sup>11</sup> Landolt-Boernstein Numerical Data and Functional Relationships in Science and Technology, Group III, Vol. 3, Edited by K. H. Hellwege, Springer-Verlag, New York, 1969; *ibid.*, Vol. 9, 1975.
- <sup>12</sup> H. W. Grueninger, R. R. Zeyfang, and M. Gauntlett, "Structural and Dielectric Properties of Lithium Niobate Solid Solutions," *Ber. Dtsch. Keram. Ges.*, **52** [7] 238–39 (1975).
- <sup>13</sup> M. Ahtee and A. M. Glazer, "Phase Transitions in Sodium Niobate-Potassium Niobate Solid Solutions," *Ferroelectrics*, **7** [1–4, Pt. 1] 93–95 (1974).
- <sup>14</sup> S. Metayer, R. V. der Muehl, J. Ravez, and P. Hagenmuller, "Effects of the Substitution of Sodium for Lithium on the Crystallographic and Dielectric Properties of Lithium Tantalate: V," *C. R. Hebd. Seances Acad. Sci., Ser. C*, **282** [17] 799–801 (1976).
- <sup>15</sup> JCPDS Powder Diffraction File, Joint Committee on Powder Diffraction Standards, Swarthmore, Pa., 1977.
- <sup>16</sup> A. F. Wells, pp. 209, 499 in *Structural Inorganic Chemistry*, 4th ed. Clarendon Press, Oxford, 1975.
- <sup>17</sup> U. Flueckinger, H. Arend, and H. R. Oswald, "Synthesis of  $\text{KNbO}_3$  Powder," *Am. Ceram. Soc. Bull.*, **56** [6] 575–77 (1977).
- <sup>18</sup> A. S. Barker, Jr. and R. Loudon, "Dielectric Properties and Optical Phonons in  $\text{LiNbO}_3$ ," *Phys. Rev.*, **158** [2] 433–45 (1967).
- <sup>19</sup> D. G. Bozins and J. P. Hurrell, "Optical Modes and Dielectric Properties of Ferroelectric Orthorhombic  $\text{KNbO}_3$ ," *Phys. Rev. B*, **13** [7] 3109–20 (1976).
- <sup>20</sup> W. L. Konijnendijk, "The Structure of Borosilicate Glasses," *Philips Res. Rep. Suppl.*, **1975**, No. 1; 243 pp.
- <sup>21</sup> W. L. Konijnendijk and J. M. Stevels, "The Structure of Borate Glasses Studied by Raman Scattering," *J. Non-Cryst. Solids*, **18** [3] 307–31 (1975).
- <sup>22</sup> W. L. Konijnendijk and J. M. Stevels, "Raman Scattering Measurements of Silicate Glasses and Compounds," *ibid.*, **21** [3] 447–53 (1976).
- <sup>23</sup> B. G. Bagley, unpublished work.
- <sup>24</sup> T. J. Negran, "A Study of the Crystallization Kinetics of Roller-Quenched  $\text{LiNbO}_3$  Glass Using Trivalent Cr Ion Luminescence as a Probe": to be published in *Physics and Chemistry of Glasses*.
- <sup>25</sup> A. M. Glass, M. E. Lines, K. Nassau, and J. W. Shiever, "Anomalous Dielectric Behavior and Reversible Pyroelectricity in Roller-Quenched  $\text{LiNbO}_3$  and  $\text{LiTaO}_3$  Glass," *Appl. Phys. Lett.*, **31** [4] 249–51 (1977).
- <sup>26</sup> A. M. Glass and K. Nassau, "Roller-Quenched Ferroelectric Oxide Glasses": in *Proceedings of the Conference on Rapid Solidification*, Nov. 13–16, Washington, D.C.
- <sup>27</sup> A. M. Glass, K. Nassau, and T. J. Negran, "Ionic Conductivity of Quenched Alkali Niobate and Tantalate Glasses," *J. Appl. Phys.*, **49** [9] 4808–11 (1978).
- <sup>28</sup> A. M. Glass and K. Nassau, "High Alkali Ion Conductivity in Rapidly Quenched Oxides Containing no Network Formers": in *Proceedings of the International Conference on Fast Ion Transport in Solids*, May 21–25, Lake Geneva, Wisconsin.

# Biaxial and Uniaxial Data for Statistical Comparisons of a Ceramic's Strength

M. N. GIOVAN\*

Jet Propulsion Laboratory, California Institute of Technology, Pasadena, California 91109

GEORGE SINES\*

University of California, Los Angeles, California 90024

The uniaxial and equibiaxial tensile strengths of a brittle material were measured in bending. Equibiaxial tension was attained by concentric ring loading of disks and uniaxial tension by four-point line loading of plates. The two specimen designs give equal volumes, surface areas, and stress gradients. Ground surfaces and lapped surfaces were tested. The equibiaxial tensile strength of a dense alumina was lower than the uniaxial tensile strengths for both ground and lapped surfaces, 8.5 and 8.1%, respectively. The Batdorf theory of flaw statistics, in which biaxial tensile strengths can be predicted from the statistical distribution of uniaxial tensile strength measurements, agreed with the data.

## I. Introduction

THERE are two classes of theories to predict the strength of brittle materials under biaxial stress. The first is derived from Griffith's flaw theory,<sup>1,2</sup> which assumes the presence of flaws of a specified shape, with enough that there is always one with the least-favorable orientation, and that crack growth from this flaw causes failure. These theories ignore the statistical nature of the problem. The second class is statistical, but it fails to specify the nature of the flaw.<sup>3</sup>

The difference between these classes is emphasized when fracture under biaxial tension is considered. According to the flaw theory, a second tensile stress at right angles gives a higher strength for open flaws or leaves it unchanged for closed flaws.<sup>2</sup> However, according to most statistical theories, there is a reduction in the strength when the transverse second tensile stress is applied. At present, weakest-link statistics have been applied only to closed flaws but in Fig. 1 the behavior which might be expected over the range from closed to circular, cylindrical, open flaws is indicated.

Presented at the 30th Pacific Coast Regional Meeting, The American Ceramic Society, Los Angeles, California, November 1, 1977 (Paper No. 11-B-77P). Received July 28, 1978; revised copy received January 8, 1979.

Supported by the National Science Foundation under Grant No. ENG-74-00138.

\*Member, the American Ceramic Society.